Bioorganic & Medicinal Chemistry 19 (2011) 4057–4066

Contents lists available at ScienceDirect

Bioorganic & Medicinal Chemistry

journal homepage: www.elsevier.com/locate/bmc

Improved therapeutic effect of folate-decorated PLGA–PEG nanoparticles for endometrial carcinoma

Changyan Liang [a,†], Yuebo Yang [a,†], You Ling [b], Yueshan Huang [b], Tian Li [a], Xiaomao Li [a,*]

[a] Department of Obstetrics and Gynecology, Third Affiliated Hospital of Sun Yat-sen University, Guangzhou 510630, China
[b] College of Bioscience and Bioengineering, South China University of Technology, Guangzhou 510640, China

ARTICLE INFO

Article history:
Received 12 March 2011
Revised 11 May 2011
Accepted 11 May 2011
Available online 18 May 2011

Keywords:
Folate receptor
PLGA nanoparticles
Endometrial carcinoma
Drug targeting
Paclitaxel

ABSTRACT

Folate (FOL) mediated poly–lactide-co-glycolide–polyethylene glycol nanoparticles (FOL–PEG–PLGA NPs) bearing paclitaxel (PTX) were prepared for the effective delivery of drug to endometrial carcinoma. The average size, zeta potential and encapsulation efficiency of FOL-targeted NPs were found to be around 220 nm, −30.43 mV and 95.6%. Cellular uptake was observed. The accumulation of FOL-targeted NPs depends on dual effects of passive and active targeting. The FOL-targeted PTX NPs showed a greater cytotoxicity against HEC-1A cancer cells in vitro and in vivo, which might be induced by apoptosis. H&E staining did not showed apparent tissue damage to liver and kidney of the mice after injecting NPs intravenously. These results suggest that the novel FOL–PEG–PLGA NPs could be a potential delivery system with excellent therapeutic efficacy for targeting the drugs to cancer cells.

1. Introduction

Endometrial cancer (EC) is the most common gynecological malignancy, with a gradual increasing incidence worldwide. An estimated 42,160 new cancer cases were diagnosed and 7780 Americans died of endometrial cancer in 2009.[1] Although most women with endometrial cancer will be diagnosed with early stage disease and have a high cure rate with surgery alone, up to 25% of women will have advanced stage or recurrent disease and require additional treatment.[2] General chemotherapy and radiotherapy offer somewhat unsatisfactory responsiveness, making new therapeutic strategies an immediate need to combat EC. Targeted cancer therapy is promising to minimize the nonspecific toxicity and to improve therapeutic efficiency compared to conventional chemotherapy.

In recent years, the design, synthesis and application of nanosized biocompatible composites have opened up new perspectives for biological and biomedical applications. Among them, the polymeric nanoparticulate drug delivery system has emerged recently as a promising carrier for targeting poorly water-soluble or amphiphilic drugs as well as genes to tumor tissues.[3] The vasculature in tumors is leaky to macromolecules, and the tumor lymphatic system is usually deficient, so nanoparticles (NPs) can be preferentially delivered to the tumor through the enhanced permeation and retention (EPR) effect via its blood vessels.[4] Still, it was found that polymeric NPs could reduce the multi-drug resistance by a mechanism of internalization of the drug and reducing its efflux from cells mediated by the P-glycoprotein.[5,6] However, it is of critical importance to develop a more specific and active system that could target to the tumor and enhance intracellular uptake of drug to the tumor site. A rational approach to achieve these goals is to exploit specific interactions between receptors on the cancer cell surface and targeting moieties conjugated to the polymer back bone.[7] Some ligands, such as folate and transferrin, can substantially increase site-specific targeting.[8,9] In particular, folate has been utilized as a targeting moiety for enhancing the therapeutic efficacy of many anticancer drugs.[10]

Folate receptor (FR) is overexpressed in several epithelial malignancies, especially in gynecological cancers, such as breast cancer, ovarian cancer, and endometrial cancer.[11,12] FR transcript has been found to be overexpressed in a significant proportion of endometrial adenocarcinoma, especially in the high-grade, high-stage tumors that are most likely to relapse.[13,14] Therefore, FR is considered to be a good candidate for tumor-specific targeting of endometrial cancer. Though there have been reported some selective targeting delivery systems, such as liposomes, that have used folate-conjugated for site-delivery of anticancer drugs,[15] there have been no reports regarding folate conjugation to NPs for targeting endometrial cancer.

In this study, we have developed folate-decorated biodegradable poly (lactide-co-glycolide) (PLGA) nanoparticles for targeted delivery by a modified solvent extraction/evaporation single emulsion method. The biodegradability and biocompatibility of PLGA

* Corresponding author. Tel./fax: +86 2085252937.
E-mail address: tigerlee_777@yahoo.cn (X. Li).
† These two authors contributed equally to this work.

0968-0896/$ - see front matter © 2011 Elsevier Ltd. All rights reserved.
doi:10.1016/j.bmc.2011.05.016

have been approved by FDA. Polyethylene glycol (PEG) is used as the coupling agent in the composition of the systems, which bridges folate with PLGA to form a chain FOL–PEG–PLGA. Paclitaxel (PTX), which is one of the first line chemotherapeutics used for the treatment of endometrial cancer,[16] is entrapped in the core of folate-decorated NPs. The characteristics of PTX/FOL–PEG–PLGA NPs, including surface morphology, particle size, drug encapsulation efficiency (EE) and in vitro release are here described. The pharmaco-dynamics of NPs are also investigated by the experiments of in vitro cellular uptake, in vitro cytotoxicity and in vivo anti-tumor activity.

2. Materials and methods

2.1. Materials

Poly (D, L-lactic-co-glycolic acid) (PLGA) (L:G molar ratio: 50:50, Mw: 15,000), *N*,*N*-dicyclohexylcarbodiimide (DCC), *N*-hydroxysuccinimide (NHS), D-α-tocopheryl polyethylene glycol 1000 succinate (TPGS), and folate were purchased from Sigma (St. Louis, MO, USA). Poly (ethylene glycol) (Mw: 3400) and dichloromethane (DCM, analytical grade) were purchased from KaiZheng Bio-technology Co. Ltd (Beijing, China). Paclitaxel (PTX) of 99.5% purity was purchased from Yunnan Hande Bio-technology Co. Ltd (Yunnan, China). 2-(4-amidinophenyl)-6-indolecarbamidine dihydrochloride (DAPI) was from Sigma–Aldrich (St. Louis, MO). DMEM medium without folate was purchased from Gibco BRL (Carlsbad, CA, USA). All other chemicals were of analytical grade.

Endometrial carcinoma cell line, HEC-1A, was obtained from ATCC (American Type Culture Collection, Manassas, VA, USA). Female nude mice (nu/nu, BALB/c mice, 4–6 weeks, body weight 17–21 g) were supplied by Guangdong Province Experimental Animal Center.

2.2. Synthesis FOL–PEG–PLGA NPs

A folate-conjugated diblock copolymer (Fig. 1A) was synthesized as follows.

Diamine-terminated poly (ethylene glycol) (H_2N–PEG–NH_2) was first prepared by the method of toluenesulfonate esterification,[17] then folate was conjugated with H_2N–PEG–NH_2 (Mw: 3400) using a modified method described elsewhere.[18,19] Folate was activated by DCC and NHS in the presence of 10 μl pyridine (folate/NHS/DCC molar ratio = 1:2:2) and reacted with 0.5 g PEG-bis-amine in 5 ml DMSO. 1.5 g of PLGA was activated by DCC and NHS in 10 ml DMSO (PLGA/NHS/DCC molar ratio = 1:1.1:1.1) at room temperature under nitrogen gas for 24 h. The final step was to conjugate FOL–PEG with activated PLGA in DMSO at room temperature for 8 h under nitrogen gas. The chemical structure of the synthesized FOL–PEG–PLGA was characterized by FTIR spectral (AXIS Ultra DLD, Kratos Instruments Corporation, UK) and ^{1}H NMR spectroscopy was used to assess the coupling of folate to the PLGA–PEG NPs.

2.3. Preparation and characterization of PTX-loaded NPs

As shown schematically in Figure 1B a modified nanoprecipitation method combined with solvent evaporation was employed in formulating PTX-loaded NPs. Briefly, FOL–PEG–PLGA or PEG–PLGA copolymer and given amount of PTX were dissolved in 5 ml DCM and vortexed for 60 s as organic phase. Then, the formed solution was slowly poured into 60 ml 0.03% (w/v) TPGS aqueous solution and sonicated with an energy output of 500 W in a continuous mode (Shanghai Kedao Ultrasonic Instrument Incorporated) for 10 min. Stirring was continued overnight to evaporate the organic solvent and allow the drug to partition into the PLGA shell. The drug-loaded NPs were separated from the unentrapped drug by washing the NPs suspension three times using an Amicon Ultra-4 centrifugal filter and freeze–dried for two days to get the NPs powder.[20,21] The fluorescent coumarin-6 and PTX were co-loaded into the nanocarrier using the same method as described above.

The concentration of PTX-loaded in NPs was measured by HPLC.[22] The mean diameter and zeta potential of the NPs were evaluated by dynamic light scanning (DLS, Mastersizer 2000, Malvern Instruments Corporation, UK). The morphology and size distribution were observed using scanning electron microscopy (SEM, Quanta 400F, Holland). To determine the in vitro drug release profile, PTX-loaded NPs were placed into a dialysis cartridge (molecular weight cut-off 3 kDa, Thermo Scientific, Rockford, IL). The cartridge was immersed in 1 L PBS and gently shaken at 100 rpm at 37 °C. At determined time intervals, the PBS solution was refreshed and the concentration of PTX remained in the dialysis cartridge was measured by HPLC.[23]

2.4. Expression of folate receptor

Expression of the folate receptor in the cells used in this study was confirmed by RT-PCR.[24] The total RNA was extracted by the Trizol reagent (Invitrogen) and cDNA was reversely transcribed in a 20 μl reaction volume using RevertAidTM First-Strand Synthesis Kit (Fermentas). PCR was then carried out with 1 μl cDNA as the template, and with the housekeeping gene β-actin as the internal control. Primers for human folate receptor were, forward: 5′-CCT GCA AAC GGC ATT TCA TC-3′ and reverse: 5′-CGG CTG TAG TTG CTG ACC TTG T-3′, and primers for β-actin (gene NW: BC016045) were, forward: 5′-ATCTGGCACCACACCTTCTACAATGGCTGCG-3′ and reverse: 5′-CATACTCCTGCTTGCTGATCCACATCTGC-3′. The abundance of RT-PCR fragments was measured by Image software.

2.5. Cellular uptake

HEC-1A cells grown on coverslips in a six-well tissue culture plate were cultured with 500 μl coumarin-6 labeled NPs at a concentration of 2 mg/mL. After incubation for 2 h, cells were washed with PBS, fixed with 5% paraformaldehyde in PBS, and stained using 5 μg/mL of DAPI for 15 min for visualization of the nuclei. The stained coverslips were photographed using confocal laser scanning microscopy (Leica TCS SP5, Germany). Coumarin-6 and DAPI showed green and blue colorations, respectively.[25]

The cellular uptake of NPs was further confirmed by flow cytometry.[26] Cells were incubated with micelles at 37 °C for 24 h, then washed and harvested by trypsinization. The pellet was resuspended in 0.5 mL of PBS for immediate analysis by Flow cytometry (FACScan, Becton Dickinson).

2.6. In vitro cytotoxicity assay

HEC-1A cells were transferred to 96-well tissue culture plates at 5000 cells per well 24 h prior to drug addition. The medium was then replaced with fresh medium containing blank and drug-loaded NPs at different concentrations. The culture medium without any drug formulations was used as the control. After 48 h, 20 μl MTT (5 μg/mL) was added to each well and incubated for 4 h at 37 °C. Medium was then removed and 150 μl DMSO was added to dissolve the blue formazan crystal converted from MTT. Cell viability was assessed by absorbance at 490 nm measured on a Bio-rad microplate reader (Bio-rad, Laboratories, USA).

2.7. Assessment of apoptosis

For morphological observation, cells were washed with cold PBS, fixed with 4% paraformaldehyde and stained with DAPI for 5 min. The stained cells were washed twice with PBS and visualized using fluorescent microscopy (Olympus, Japan). Percentage of apoptosis

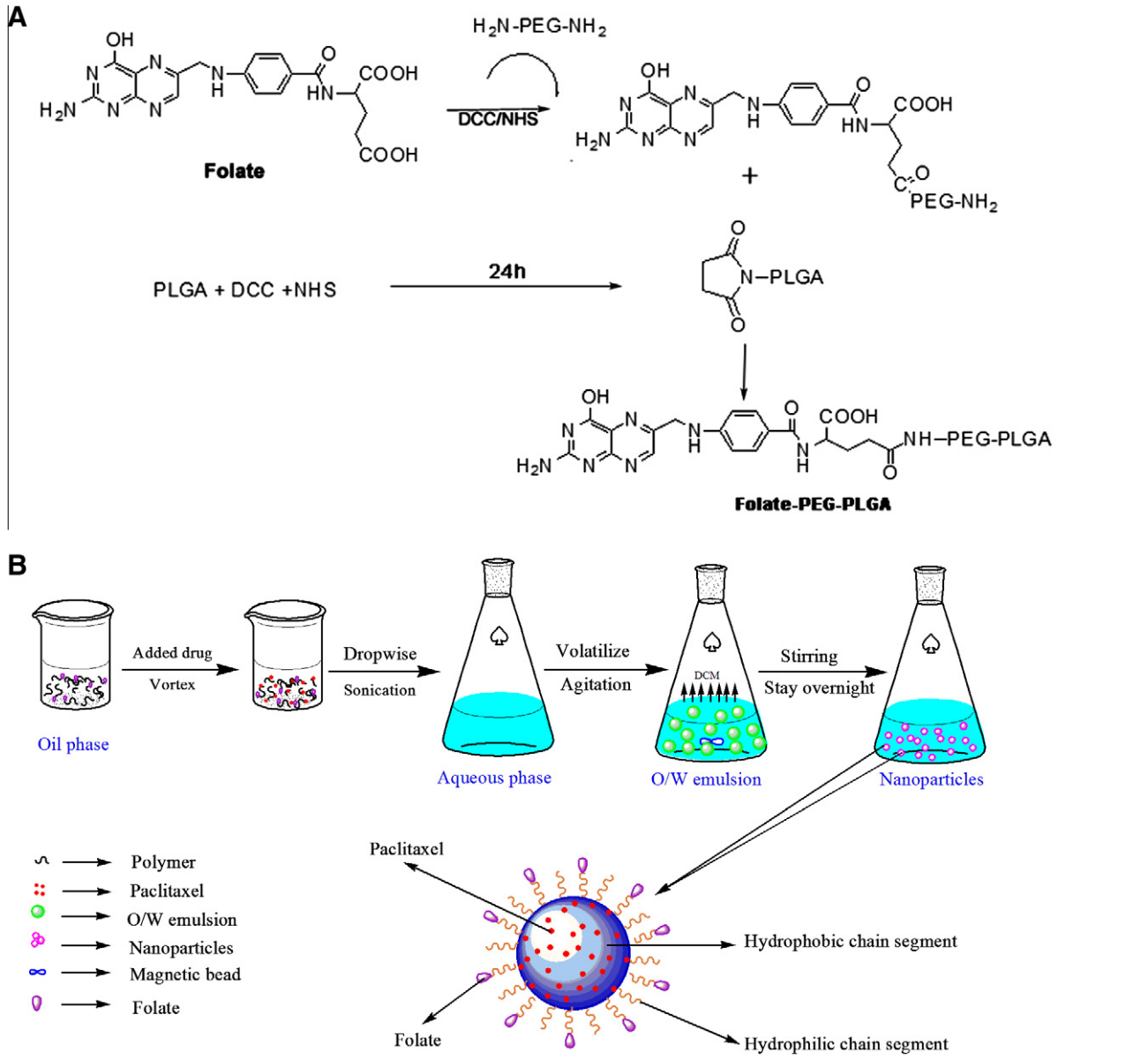

Fig. 1. (A) Structure of FOL–PEG–PLGA. (B) Schematic representing formulation of FOL–PEG–PLGA nanoparticles and the process for drug loading.

was calculated by counting the condensed and fragmented nuclei in cells.[27] The experiment was repeated three times.

For detection of apoptosis, cells were stained with Annexin-V FITC and propidium iodide (PI). In brief, the cells were pretreated with PTX–NPs or free PTX at equivalent drug concentrations (2 μg/mL). After suspending the specimens in 200 μl of binding buffer, 10 μl of Annexin V-FITC and 5 μl of PI were added to the cell suspension and incubated for 15 min in dark at room temperature. Another 300 μl of binding buffer was added and then analyzed by a FACScan flow cytometer using a FACS Calibu. Cells undergoing early apoptosis bind only to Annexin V, and cells that bind both to Annexin V and PI are either in the late stages of apoptosis or already dead. The experiment was repeated three times.

2.8. Assessment of anti-tumor activity in vitro

The anti-tumor efficacy of the drug-loaded NPs was assessed in tumor-bearing mice. The subcutaneous dorsa of BALB/c nude mice were inoculated with 1×10^7 HEC-1A cells in 100 μl of normal saline. When the average volume of the xenografts tumor was approximately 70 mm^3, the mice were randomly divided into four groups with six mice in each group. Group A was given—normal saline, group B—free PTX, group C-PTX/PLGA–PEG NPs and group D-PTX/FOL–PEG–PLGA NPs. Various formulation of PTX (at the same drug concentration of 5 mg/kg) was injected intravenously via the tail vein every two days for a total of four times, and the mice were then observed for 18 days. The tumor diameters were measured every three days for each tumor-bearing mouse. The tumor volume (V) was calculated as:[28] $V = [\text{length} \times (\text{width})^2]/2$. The tumor, liver and kidney tissues of were H&E stained for observation of the effect of the NPs on mice organs.

3. Results and discussion

3.1. Synthesis of FOL–PEG–PLGA

The principle of the chemical reactions in synthesis of FOL–PEG–PLGA is the formation of amide bonds. The conjugate structure was checked and confirmed by FTIR and ^1H NMR spectroscopy as shown in Figure 2. FTIR spectrum (Fig. 2A) quantitatively

assessed the conjugation by several characteristic vibrational modes. More specifically, the bands at ~1535 cm^{-1} and 1627 cm^{-1} were assigned to C–O–C ether stretching vibration of NH_2–PEG–NH_2 and –COO stretching vibration of PLGA, respectively. The band around 1573 cm^{-1} was attributed to characteristic absorption band of the phenyl ring in folic acid. ^1H NMR analysis (Fig. 2B) showed principal peaks (in ppm) related to benzene of folate moiety [δ = 6.64, 6.90, 7.65, 7.87 ppm], the PEG moiety [δ = 3.41 ppm], and the PLGA moiety [δ = 5.01–4.71 ppm]. All these results demonstrated successful introduction of folate into the backbone of diblock copolymer PLGA–PEG to form a conjugate.

3.2. Characterization of PTX/FOL–PEG–PLGA NPs

SEM measurement showed that the mean diameter of PLGA–PEG NPs was around 204 ± 2.1 nm, with a polydispersity index of 0.093, and the mean diameter of targeted micelles was 220.4 ± 3.0 nm, with a polydispersity index 0.113 (Fig. 3A). The particle sizes increase of the targeted micelles presumably owed to the presence of folate fragment on the micelles surface. SEM micrographs revealed that the NPs had a spherical morphology and smooth surface (Fig. 3B).

Surface zeta potential is closely related to the stability of NPs. High surface potential of the suspension system of NPs can reduce the cohesion between particles, thereby resulting in high stability.[29–31] We found that the folate-decorated PLGA NPs had a lower negative charge of −8.02 ± 0.54 mV, comparing with the surface charge of −27.98 ± 1.44 mV of the PLGA–PEG NPs. It is possible that the protonated amino acid groups of folate minimize carboxylic acid groups of the polymer present on the surface of PLGA particles. In our study, D-sorbitol was used to increase the surface zeta potential of folate-conjugated NPs from −8.02 ± 0.54 mV to −30.43 ± 4.55 mV. This may be due to the increase of the alcoholic hydroxyl negative ion of nanoparticles by D-sorbitol.[32–34]

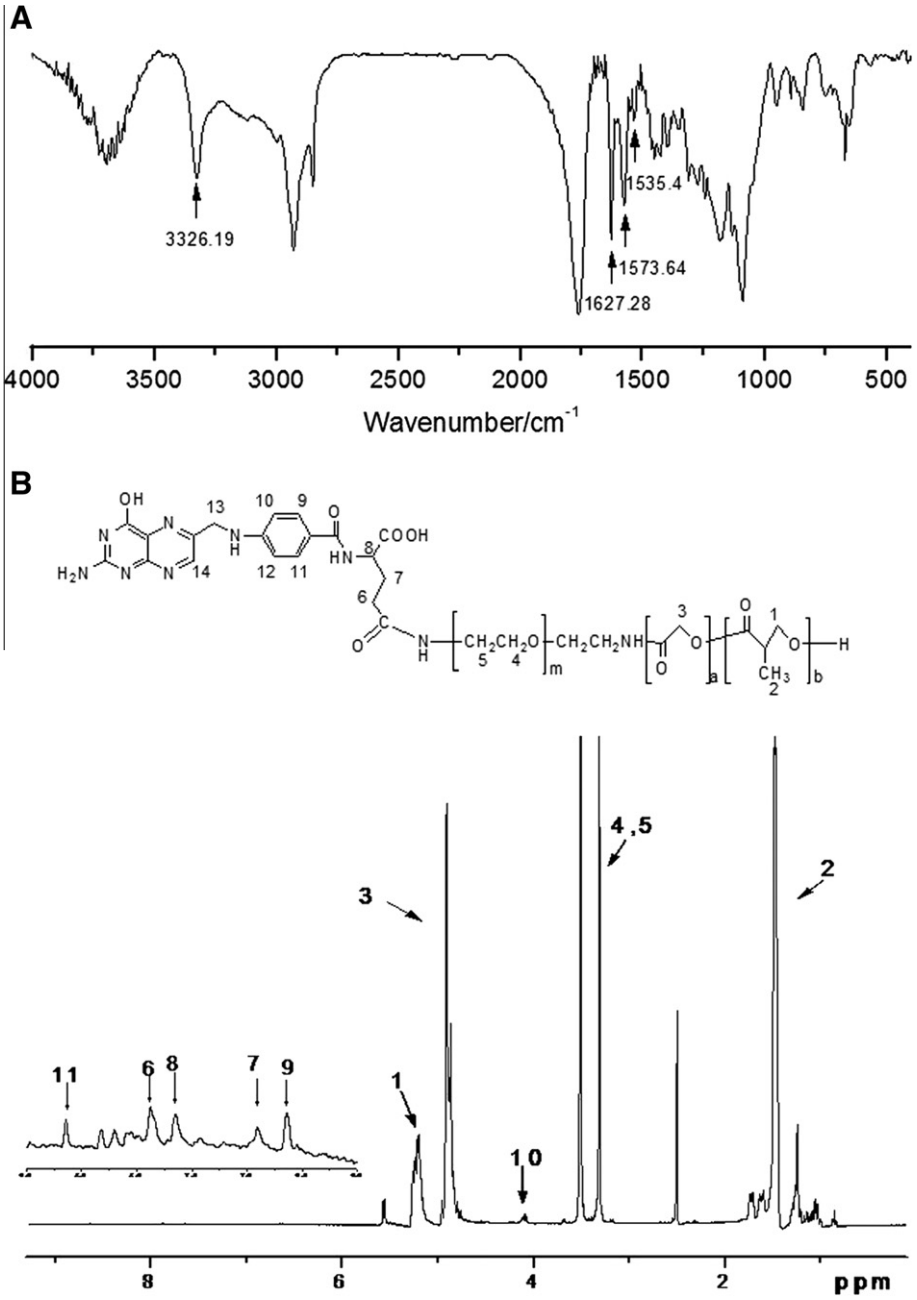

Fig. 2. The FTIR spectrum (A) and ^1H NMR spectrum (B) of FOL–PEG–PLGA.

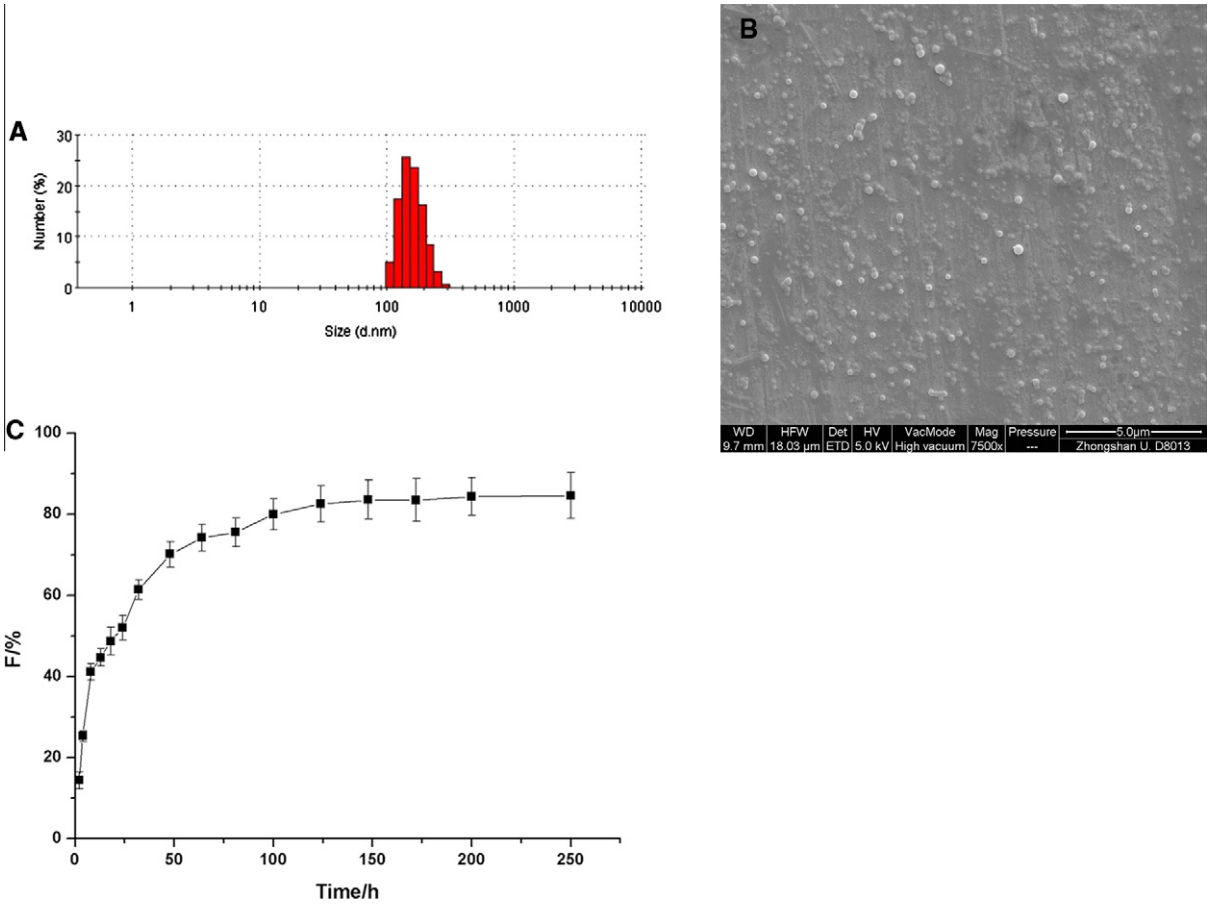

Fig. 3. Characterization of PTX/FOL–PEG–PLGA nanoparticles: (A) Size distribution spectrum; (B) SEM image; (C) drug release profile determined by a dialysis method in vitro.

The effects of emulsifier concentration and aqueous to organic phase ratio (w/o, v/v) on the encapsulation efficiency were investigated. The TPGS is comprised of lipophilic alkyl tail and hydrophilic polar head, so the addition of emulsifier can be expected to increase the entrapment efficiency of paclitaxel dissolved in the organic phase. During synthesis, with increase of aqueous to organic phase ratio, the entrapment efficiency of paclitaxel increased first and then decreased slightly. That is probably because with the gradual increase of w/o ratio, milk drops in the aqueous phase can be fully dispersed and particles yield greater access to higher encapsulation efficiency. However, when the w/o reached a cut-off ratio, the particle size became smaller, and PTX may disperse into the aqueous phase and deposit, which can reduce the loading efficiency of paclitaxel. Base on these findings, the TPGS concentration of 0.03% and aqueous to organic phase ratio of 0.27 were identified as parameters for the optimal formulation. The encapsulation efficiency under this optimal formulation was 95.6%.

Using a membrane dialysis method, both PTX/PLGA–PEG and PTX/FOL–PEG–PLGA NPs were found to exhibit sustained drug release into surrounding PBS, with rapid release of 20% of the drug in the first 2 h, and a cumulative release of 40% of the drug by 12 h, followed by a slow linear release of 80% of the drug by 150 h. The initial rapid release of drug could be due to the release of some loosely bound drugs on the surface of the nanoparticles by a mechanism of diffusion. This initial release was later followed by more controlled release during the two-week study period (Fig. 3C), which was a result of the degradation of the polymer.

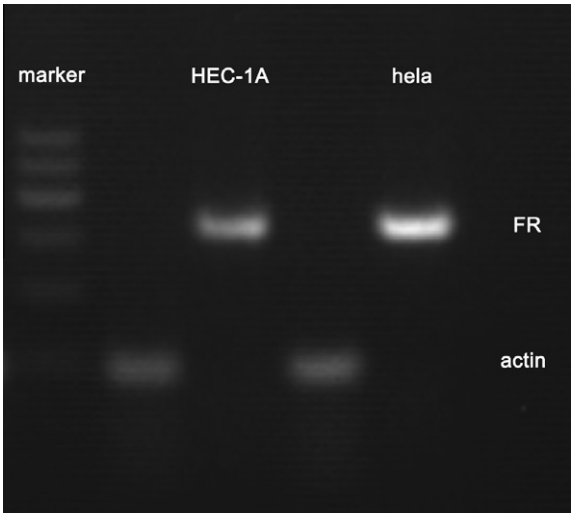

Fig. 4. Typical gel electrophoresis images of the expression of folate receptor in HEC-1A cells, a human endometrial carcinoma cell line. Hela cells, a human cervical cell line were as a positive control. The primers used for hFR and action were specific to the respective genes.

3.3. Expression of folate receptor on HEC-1A and cellular uptake of nanoparticles

The presence of folate receptor in the cell line used was confirmed by RT-PCR. The human cervical carcinoma cell line hela is

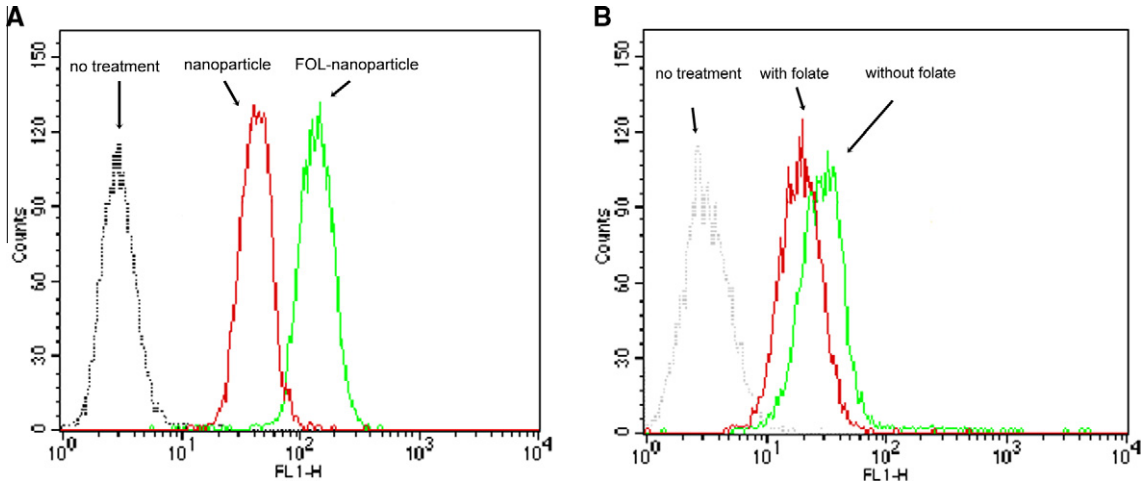

Fig. 5. Uptake of the nanoparticles by HEC-1A cells. Cells were treated with coumarin-6-labeled nanoparticles with or without folate modified and cellular fluorescence was measured by flow cytometry. Results are shown in histogram with the X-axis indicating the cellular fluorescence intensity and the Y-axis indicating the cell count. (A) Cells treated with the nanoparticles and the FOL-nanoparticles and (B) cells treated with the FOL-nanoparticles were cultured in media with or without 2 nM folate.

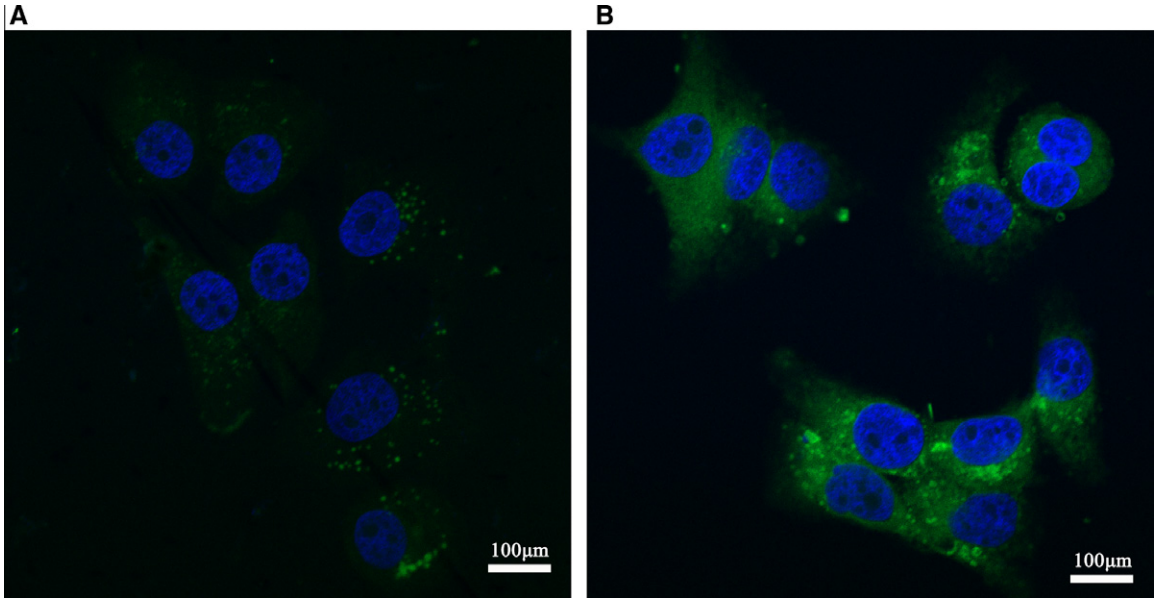

Fig. 6. Confocal laser scanning microscopy (CLSM) of HEC-1A cancer cells incubated with coumarin-6 labeled nanoparticles in the medium for 2 h. Coumarin-6 and DAPI showed green and blue colorations, respectively. (A) PLGA–PEG nanoparticles; (B) FOL–PEG–PLGA nanoparticles.

Table 1
Cytotoxicity of PTX/PLGA–PEG–FOL NPs in HEC-1A cells determined by MTT assay

Group	IC_{50} (μg/mL)
Free PTX	13.24 ± 1.59
PTX/PLGA–PEG NPs	8.81 ± 0.10
PTX/PLGA–PEG–FOL NPs	3.43 ± 0.28

known to be rich of FR-α mRNA expression. As gel electrophoresis images shown (Fig. 4) both HEC-1A and hela cells have a high-level FR-α mRNA expression.

Flow cytometry analysis was performed to compare cellular uptake of nanoparticles for the desired time. Since the free coumarin-6 has been centrifuged and washed with PBS previously, the fluorescence intensity is proportional to the amount of the NPs internalized by the cells. Histograms of cell-associated coumarin-6

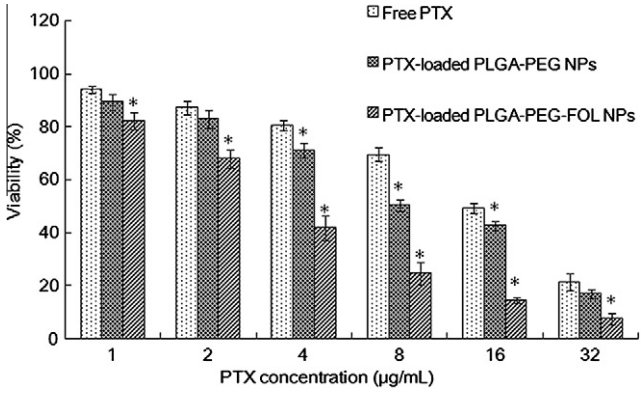

Fig. 7. Cytotoxicity of PTX NPs formulations vs free PTX after 48 h incubation time on HEC-1A cancer cell lines. (*p <0.05, data is presented as mean ± S.D., n = 3).

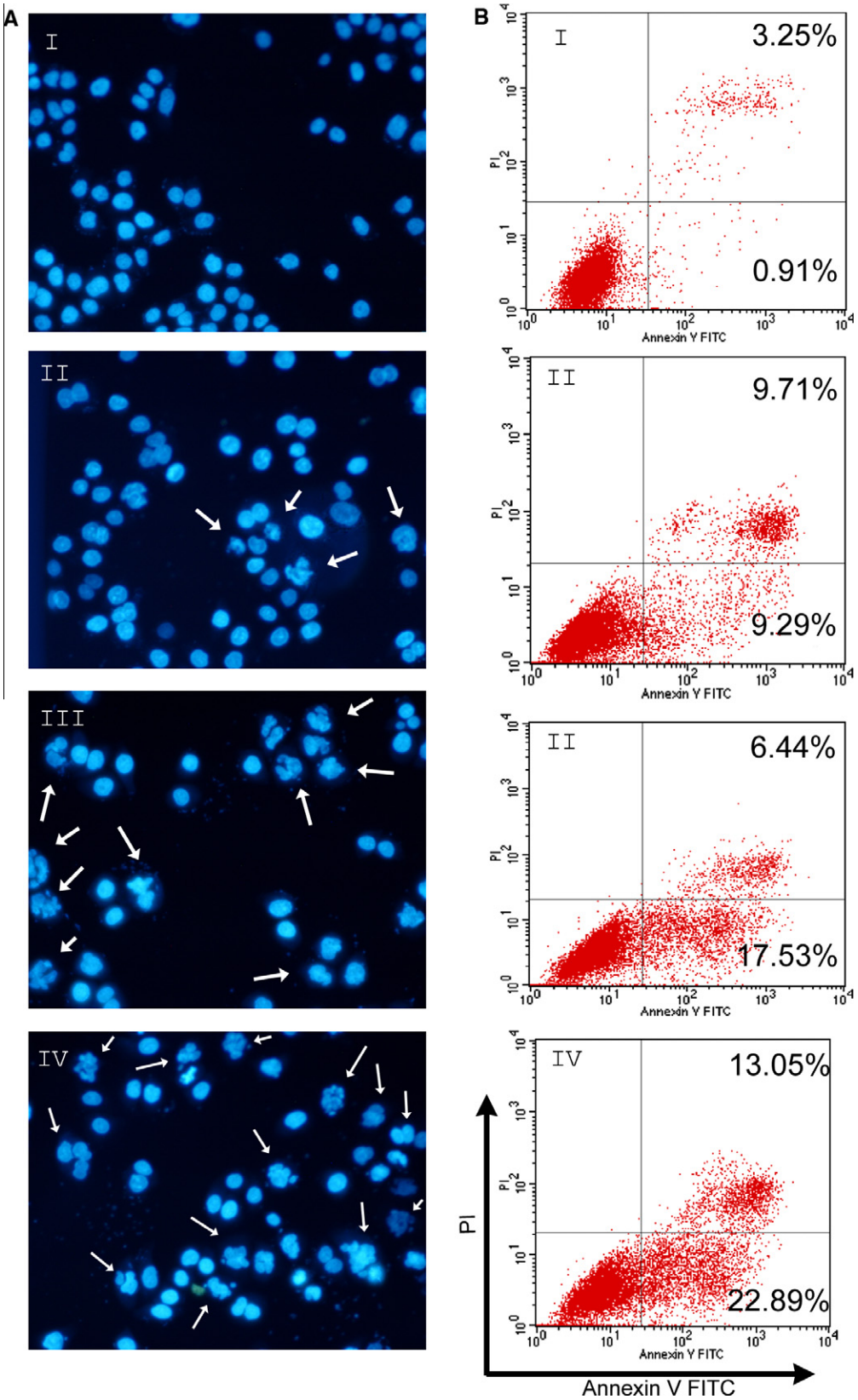

Fig. 8. (A) Representative microphotographs of DAPI staining. HEC-1A cells were treated with free PTX and PTX–NPs at equivalent drug concentration (2 μg/ml) for 48 h followed by visualization of DNA staining with DAPI using a fluorescence microscope. (I) control, (II) free PTX, (III) PTX/PLGA–PEG NPs, (IV) PTX/FOL–PEG–PLGA NPs. Representative of four individual experiments ($n = 3$). (B) The cells were treated with free PTX, PTX/PLGA–PEG NPs and PTX/FOL–PEG–PLGA NPs at equivalent drug concentration for 48 h and analyzed for apoptosis by flow cytometry. The Annexin-V + PI apoptotic cells shown for each histogram are for one experiment representative of the three performed. The fluorescence of PI is expressed in channel numbers (In the dot plots, cells in early apoptosis: bottom right quadrant and cells in late apoptosis: top right quadrant are shown).

fluorescence from HEC-1A cells are shown in Figure 5. Cells without NPs treatment were used as the negative control, and showed only the auto-fluorescence of the cells. With equivalent coumarin-6 concentration in each formulation and the same incubation time, the coumarin-6-loaded targeted NPs showed markedly higher fluorescence intensity than non-targeted NPs (Fig. 5A). However, the presence of 2 nM of folate in the culture medium (Fig. 5B) drastically suppressed the fluorescence intensity of HEC-1A cells, which indicated that the presence of folate significantly inhibited the uptake of FOL-targeted NPs in FR (+) cells. These results directly demonstrated that the cellular uptake of the micelles can be enhanced by FOL-receptor mediated endocytosis process, which are consistent with previous reports regarding FOL-receptor-dependent cellular uptake of folate-conjugated polymeric micelles for anticancer therapy.[35,36]

To investigate the effect of FR on cellular uptake, the extent of cellular uptake of coumarin-6-labeled NPs by HEC-1A cells was also evaluated by CLSM. Cells were incubated with FOL-free culture medium containing coumarin-6-labeled FOL–PEG–PLGA NPs or PLGA–PEG NPs (all or equivalent coumarin-6 concentrations). All observations were conducted under identical operating conditions. As shown in Figure 6, after 2 h of incubation, detectable green fluorescence was observed in the cytoplasm of the cell, and the nucleus of the cell was stained blue with DAPI without any green fluorescence, which indicated that the NPs was mainly uptaken into the cytoplasm. Cells treated with coumarin-6-labeled FOL–PEG–PLGA NPs had very strong green fluorescence, but in contrast, cells incubated with FOL-ree PLGA–PEG NPs showed weak green fluorescence. These results further indicate that the cellular uptake of the coumarin-6-labeled FOL–PEG–PLGA NPs is mainly based on a FOL-receptor mediated endocytosis mechanism that might result in a greater amount of NPs internalized inside tumor cells.[37–39] The FOL-free coumarin-6-labeled PLGA NPs might be taken up by the cells through a nonspecific endocytosis mechanism.

3.4. In vitro anti-tumoral activity

The cell viability (%) in the presence of blank PLGA NPs and blank FOL–PEG–PLGA NPs (100 μg/ml) was 99.9 ± 2.8% and 103 ± 1.6%. The results demonstrated the two blank NPs had no significant cytotoxic effect on cells even at doses as high as 100 μg/ml and the two polymers displayed satisfactory biocompatibility. Drug-loaded nanoparticles, PTX/PLGA–PEG NPs and PTX/FOL–PEG–PLGA NPs with varied drug-loading levels and amounts were added to HEC-1A cells to evaluate the inhibition effect on the cells. Table 1 summarized the IC_{50} values of nanoparticulate formulations and free drug under conditions of light irradiation. The PTX–NPs showed significant advantages in inhibiting cancer cell proliferation compared to PTX in solution (p <0.05). The amount of PTX required to achieve 50% of growth inhibition (IC_{50}) was much lower in FOL coupled nanoparticles than in solution (13.24 ± 1.59 μg/mL and 3.43 ± 0.28 μg/mL, respectively). The FOL coupled nanoparticles enhanced the cytotoxicity of PTX about 3.9-fold on HEC-1A cell compared with the PTX solution. Due to the multi-drug resistance effect, the free drug outfluxing through p-glycoprotein resulted in a decrease in intracellular concentration of the drug.[40] As a greater amount of drug could be delivered into cells in the form of NPs by endocytosis, the cells were more vulnerable to the cytotoxic effect of the drug. The therapeutic action of targeted micelles had a better cell inhibition efficiency to HEC-1A cells than that of non-targeted micelles system (p <0.05). This result is considered to be due to the enhanced receptor-mediated internalization mediated by FOL ligand.[41] For example, after being treated with PTX of the equivalent concentration (16 μg/ml), the viability of HEC-1A cells treated with PTX/ FOL–PEG–PLGA NPs was 14.78% compared with that of 42.62% of HEC-1A cells treated with PTX/PLGA–PEG NPs (Fig. 7).

3.5. PTX–NPs increased the PTX-induced apoptosis in HEC-1A cells

Previous studies in a variety of cancer cells have shown that the anticancer properties of paclitaxel are caused in part by initiation of the apoptotic cascade.[42] cell growth and morphologic studies (Fig. 8A) showed that the HEC-1A cells without treatment displayed normal nuclear morphology, whereas DNA fragmentation and/or chromatin condensation was frequently observed in cells treated with PTX or PTX–NPs, indicating that PTX or PTX–NPs induced apoptosis. Flow cytometry was also used to measure the fraction of apoptotic cells following administration of either PTX or PTX–NPs with the equivalent PTX concentration of 2 μg/ml at 48 h. As shown in graph in Figure 8B, free PTX, PTX/PLGA–PEG NPs and PTX/FOL–PEG–PLGA NPs caused 19%, 23.97% and 35.94% apoptosis in HEC-1A cells, respectively. The PTX/ FOL–PEG–PLGA NPs treatment resulted in a significant increase in the proportion of apoptotic cells compared with PTX, which was consistent with the data from cytotoxic analysis.

3.6. In vivo anti-tumor activity

To assess anti-tumor activity in vivo, a tumor regression study was carried out. Normal saline, free PTX, PTX/PLGA–PEG and targeted micelles were injected through the tail vein to mice bearing endometrial carcinoma HEC-1A cells at clinically relevant doses. Significant anti-tumor effect was observed in groups of free PTX and drug-loaded micelles compared with the normal saline group (p <0.05). Owing to sustained release behavior of PTX-loaded NPs, the tumor volumes of NP-treated groups were smaller than that of free PTX that has a shorter half-life. As showed in Figure 9, by 18 days after the final administration, the average tumor volume in PTX-loaded NP-treated mice gradually reduced to about 692 and 475 mm^3, while the average tumor volume in normal saline-treated mice was 1315 mm^3. The PTX-loaded FOL-targeted NPs showed a significantly higher anti-tumor efficacy than free PTX, with a final mean tumor load of 474.88 ± 151.46, remarkably smaller than other treated groups (p <0.05). The inhibition rate of targeted NPs was 63.90%, higher than that of 47.42% of non-targeted NPs (p <0.05). This result is consistent with our previous study in cells. Targeted micelles delivery may involve two phases. In the first phase, micelles slowly accumulate in tumor tissue,

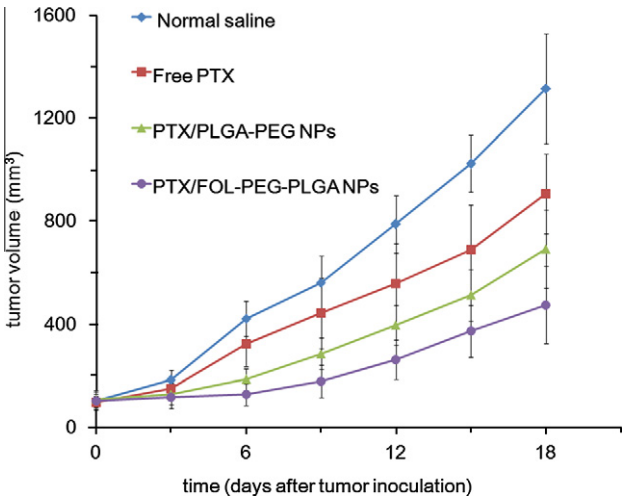

Fig. 9. Tumor volume changes of BALB/C nude mice bearing HEC-1A tumors after intravenous injections of various formulations of PTX (n = 6).

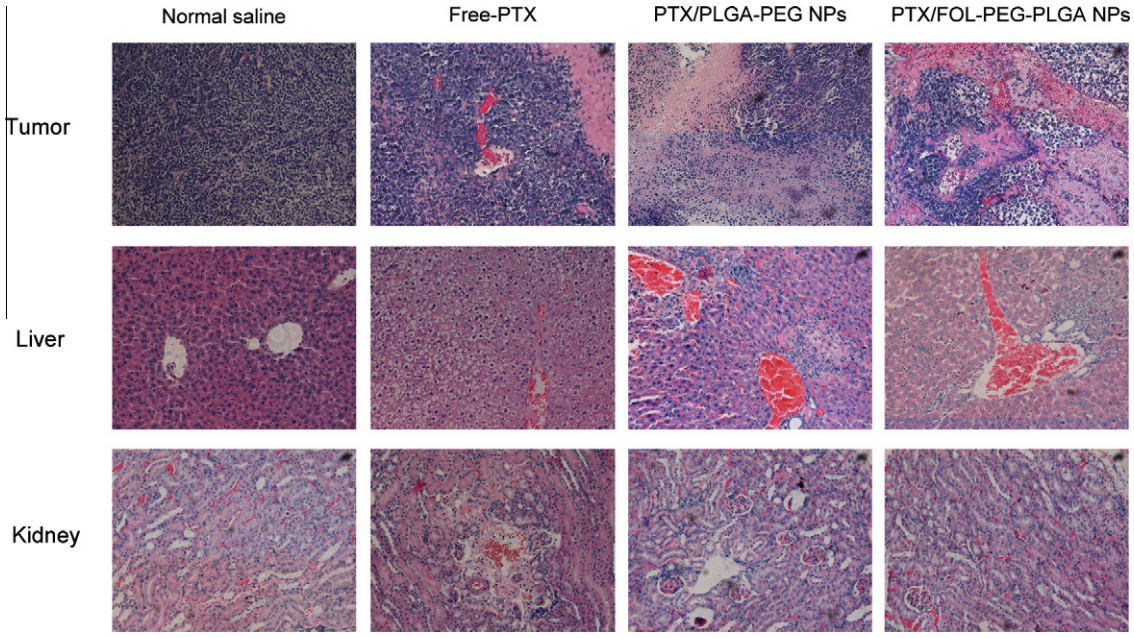

Fig. 10. Histopathological findings of the tissue of mice by 18 days after administration of different formulation of PTX. H&E staining revealed the morphology and structure of tumor, liver and kidney in normal saline group, free PTX group, PTX/PLGA–PEG group and PTX/FOL–PEG–PLGA group (magnification, 200×).

ultimately reaching high levels due to the EPR effect. In the second phase, non-decorated micelles remain in the interstitial space and are subject to decomposition, degradation, or phagocytosis, resulting in release of the drug. In contrast, targeted micelles bind to and internalize in the tumor cells via ligand–receptor interactions, resulting in a potent anti-tumor activity.[25] In this study, the PTX-loaded FOL-targeted micelles obviously showed the highest anti-tumor efficacy.

H&E staining of the tissue sections was conducted for observation of the tissues change following drug administration (Fig. 10). The normal saline group showed typical pathological features of the tumor, rich of cells with enlarged and deeply stained nuclei, irregular shape, and little cytoplasm. The other groups with different drug loading treatment, especially in the PTX/FOL–PEG–PLGA treated group, varying degree of tumor necrosis was observed, with much fewer cancer cells, which showed shrunken nuclei and increased cytoplasm. It is obvious that the targeted micelles can better accumulate in the tumor tissue and kill cancer cells. One thing that needs to note is that he particles mainly accumulate in the liver following phagocytosis,[43] and liver toxicity is one of the serious side effects of paclitaxel in clinical application, which can cause fatty degeneration or necrosis.[44] Liver staining in the free PTX group showed hydropic degeneration and fatty degeneration, while in the nanoparticles treated groups, no significant liver cell damage was observed, but with slightly inflammatory cell infiltration. The general morphology of the kidneys of the nude mice treated with drug-loaded nanoparticles was normal, maintaining the glomerular structural integrity, while slight inflammatory cell infiltration was seen in the kidneys of free PTX-treated mice.

4. Conclusions

In this study, we have synthesized an FOL–PEG–PLGA conjugate and confirmed its chemical structure by FTIR and ^{1}H NMR spectroscopy. PTX/FOL–PEG–PLGA NPs have been used for targeting delivery of PTX to endometrial carcinoma HEC-1A cells. We have found that the PTX/FOL–PEG–PLGA NPs have greatly increased the tumor targeting efficiency and specificity, and showed significantly better anticancer effect than the free drug only group. This study has reported a novel technique for the preparation of PTX/FOL–PEG–PLGA NPs, and their application in selective delivery of anticancer drug to the FR-overexpressed cancer cells, which has opened a new vista for site-specific targeting for anticancer therapy.

Acknowledgment

We are grateful to the financial support from Guangzhou Municipal Science and Technology Program (Grant no. 2007Z3-E0601), Guangdong province Science and Technology Program (Grant no. 2007B030502014) and National Natural Science Foundation of China (Grant no. 30772332).

Supplementary data

Supplementary data associated with this article can be found, in the online version, at doi:10.1016/j.bmc.2011.05.016. These data include MOL files and InChiKeys of the most important compounds described in this article.

References and notes

1. Jemal, A.; Siegel, R.; Ward, E.; Hao, Y.; Xu, J.; Thun, M. J. *CA Cancer J. Clin.* **2009**, *59*, 225.
2. Shafer, A.; Zhou, C.; Gehrig, P. A.; Boggess, J. F.; Bae-Jump, V. L. *Int. J. Cancer* **2010**, *126*, 1144.
3. Wang, X.; Yang, L.; Chen, Z. G.; Shin, D. M. *CA Cancer J. Clin.* **2008**, *58*, 97.
4. Matsumura, Y.; Maeda, H. *Cancer Res.* **1986**, *46*, 6387.
5. Li, N.; Yang, X.; Zhai, G.; Li, L. *J. Colloid Interf. Sci.* **2010**, *350*, 117.
6. Patil, Y.; Sadhukha, T.; Ma, L.; Panyam, J. *J. Control Release* **2009**, *136*, 21.
7. Allen, T. M. *Nat. Rev. Cancer* **2002**, *2*, 750.
8. Zheng, Y.; Yu, B.; Weecharangsan, W.; Piao, L.; Darby, M.; Mao, Y.; Koynova, R.; Yang, X.; Li, H.; Xu, S.; Lee, L. J.; Sugimoto, Y.; Brueggemeier, R. W.; Lee, R. J. *Int. J. Pharm.* **2010**, *390*, 234.
9. Zhang, Z.; Jia, J.; Lai, Y.; Ma, Y.; Weng, J.; Sun, L. *Bioorg. Med. Chem.* **2010**, *18*, 5528.
10. Salazar, M. D.; Ratnam, M. *Cancer Metastasis Rev.* **2007**, *26*, 141.
11. Hartmann, L. C.; Keeney, G. L.; Lingle, W. L.; Christianson, T. J.; Varghese, B.; Hillman, D.; Oberg, A. L.; Low, P. S. *Int. J. Cancer* **2007**, *121*, 938.
12. Basal, E.; Eghbali-Fatourechi, G. Z.; Kalli, K. R.; Hartmann, L. C.; Goodman, K. M.; Goode, E. L.; Kamen, B. A.; Low, P. S.; Knutson, K. L. *PLoS ONE* **2009**, *4*, e6292.
13. Maxwell, G. L.; Chandramouli, G. V.; Dainty, L.; Litzi, T. J.; Berchuck, A.; Barrett, J. C.; Risinger, J. I. *Clin. Cancer Res.* **2005**, *11*, 4056.
14. Dainty, L. A.; Risinger, J. I.; Morrison, C.; Chandramouli, G. V.; Bidus, M. A.; Zahn, C.; Rose, G. S.; Fowler, J.; Berchuck, A.; Maxwell, G. L. *Gynecol. Oncol.* **2007**, *105*, 563.

15. Wu, J.; Liu, Q.; Lee, R. J. *Int. J. Pharm.* **2006**, *316*, 148.
16. Gadducci, A.; Cosio, S.; Genazzani, A. R. *Crit. Rev. Oncol. Hematol.* **2006**, *58*, 242.
17. Wang, L.; Shi, J.; Kim, Y. S.; Zhai, S.; Jia, B.; Zhao, H.; Liu, Z.; Wang, F.; Chen, X.; Liu, S. *Mol. Pharm.* **2009**, *6*, 231.
18. Yoo, H. S.; Park, T. G. *J. Control Release* **2001**, *70*, 63.
19. Yoo, H. S.; Lee, K. H.; Oh, J. E.; Park, T. G. *J. Control Release* **2000**, *68*, 419.
20. Sheng, Y.; Liu, C.; Yuan, Y.; Tao, X.; Yang, F.; Shan, X.; Zhou, H.; Xu, F. *Biomaterials* **2009**, *30*, 2340.
21. Coombes, A. G.; Yeh, M. K.; Lavelle, E. C.; Davis, S. S. *J. Control Release* **1998**, *52*, 311.
22. Gomez-Gaete, C.; Tsapis, N.; Besnard, M.; Bochot, A.; Fattal, E. *Int. J. Pharm.* **2007**, *331*, 153.
23. Lee, M. K.; Lim, S. J.; Kim, C. K. *Biomaterials* **2007**, *28*, 2137.
24. Paranjpe, P. V.; Chen, Y.; Kholodovych, V.; Welsh, W.; Stein, S.; Sinko, P. J. *J. Control Release* **2004**, *100*, 275.
25. Jin, C.; Qian, N.; Zhao, W.; Yang, W.; Bai, L.; Wu, H.; Wang, M.; Song, W.; Dou, K. *Biomacromolecules* **2010**, *11*, 2422.
26. Lin, J. J.; Chen, J. S.; Huang, S. J.; Ko, J. H.; Wang, Y. M.; Chen, T. L.; Wang, L. F. *Biomaterials* **2009**, *30*, 5114.
27. Luo, Y.; Ling, Y.; Guo, W.; Pang, J.; Liu, W.; Fang, Y.; Wen, X.; Wei, K.; Gao, X. *J. Control Release* **2010**, *147*, 278.
28. Park, J.; Fong, P. M.; Lu, J.; Russell, K. S.; Booth, C. J.; Saltzman, W. M.; Fahmy, T. M. *Nanomedicine* **2009**, *5*, 410.
29. Singh, R.; Lillard, J. J. *Exp. Mol. Pathol.* **2009**, *86*, 215.
30. Yan, F.; Zhang, C.; Zheng, Y.; Mei, L.; Tang, L.; Song, C.; Sun, H.; Huang, L. *Nanomedicine* **2010**, *6*, 170.
31. Win, K. Y.; Feng, S. S. *Biomaterials* **2006**, *27*, 2285.
32. Xue, C. H.; Zhou, R. J.; Shi, M. M.; Gao, Y.; Wu, G.; Zhang, X. B.; Chen, H. Z.; Wang, M. *Nanotechnology* **2008**, 19.
33. Wang, A.; Yin, H.; Lu, H.; Xue, J.; Ren, M.; Jiang, T. *Langmuir* **2009**, *25*, 12736.
34. Schilling, C. H.; Sikora, M.; Tomasik, P.; Li, C.; Garcia, V. *J. Eur. Ceram. Soc.* **2002**, *22*, 917.
35. Hattori, Y.; Maitani, Y. *Cancer Gene Ther.* **2005**, *12*, 796.
36. Yoo, H. S.; Park, T. G. *J. Control Release* **2004**, *100*, 247.
37. Hattori, Y.; Maitani, Y. *Curr. Drug Deliv.* **2005**, *2*, 243.
38. Alexis, F.; Basto, P.; Levy-Nissenbaum, E.; Radovic-Moreno, A. F.; Zhang, L.; Pridgen, E.; Wang, A. Z.; Marein, S. L.; Westerhof, K.; Molnar, L. K.; Farokhzad, O. C. *ChemMedChem* **2008**, *3*, 1839.
39. Emerich, D. F.; Thanos, C. G. *J. Drug Target.* **2007**, *15*, 163.
40. Jain, A.; Jain, S. K. *Eur. J. Pharm. Sci.* **2008**, *35*, 404.
41. Shen, Z.; Li, Y.; Kohama, K.; Oneill, B.; Bi, J. *Pharmacol. Res.* **2010**.
42. Kutuk, O.; Letai, A. *Cancer Res.* **2008**, *68*, 7985.
43. Avgoustakis, K.; Beletsi, A.; Panagi, Z.; Klepetsanis, P.; Livaniou, E.; Evangelatos, G.; Ithakissios, D. S. *Int. J. Pharm.* **2003**, *259*, 115.
44. Ohe, Y.; Niho, S.; Kakinuma, R.; Kubota, K.; Matsumoto, T.; Ohmatsu, H.; Goto, K.; Kunitoh, H.; Saijo, N.; Nishiwaki, Y. *Jpn. J. Clin. Oncol.* **2001**, *31*, 100.